Journal of Power Sources 192 (2009) 582–587

Contents lists available at ScienceDirect

Journal of Power Sources

journal homepage: www.elsevier.com/locate/jpowsour

Catalytic effect of titanium nitride nanopowder on hydrogen desorption properties of $NaAlH_4$ and its stability in $NaAlH_4$

Ji Woo Kim[a,b,c], Jae-Hyeok Shim[b,*], Seul Cham Kim[a], Arndt Remhof[c], Andreas Borgschulte[c], Oliver Friedrichs[c], Robin Gremaud[c], Flavio Pendolino[c], Andreas Züttel[c], Young Whan Cho[b], Kyu Hwan Oh[a]

[a] Department of Materials Science and Engineering, Seoul National University, Seoul 151-742, Republic of Korea
[b] Materials Science and Technology Research Division, Korea Institute of Science and Technology, Seoul 136-791, Republic of Korea
[c] Division of Hydrogen and Energy, Department of Environment, Energy and Mobility, Empa Materials Science and Technology, CH-8600 Dübendorf, Switzerland

ARTICLE INFO

Article history:
Received 24 November 2008
Received in revised form 13 January 2009
Accepted 6 February 2009
Available online 13 March 2009

Keywords:
Hydrogen storage
Sodium alanate
Catalyst
Titanium nitride nanopowder
In situ X-ray diffraction
In situ Raman spectroscopy

ABSTRACT

Single crystalline titanium nitride (TiN) nanopowder is synthesized by a mechano-chemical reaction between titanium chloride ($TiCl_3$) and lithium nitride (Li_3N) by means of high-energy ball milling. The TiN nanopowder has an average particle size of 6 nm and is introduced into sodium alanate ($NaAlH_4$) as a catalyst. During hydrogen sorption cycles, TiN-catalyzed $NaAlH_4$ exhibits a greater hydrogen desorption rate and higher hydrogen capacity than $TiCl_3$-catalyzed $NaAlH_4$. Contradicting thermodynamic predictions, in situ X-ray diffraction results reveal that TiN nanopowder remains stable and produces no by-products (e.g., Ti–Al compounds) in the reaction with $NaAlH_4$ during hydrogen desorption. In situ Raman spectroscopy also confirms the stability of TiN nanopowder in $NaAlH_4$. This implies that the sustained hydrogen sorption kinetics and hydrogen capacity of TiN-catalyzed $NaAlH_4$ originate from the structural and chemical stability of TiN nanopowder in $NaAlH_4$ for the given conditions of the hydrogen cycle test.

1. Introduction

Hydrogen as a future energy carrier requires adequate storage materials that can satisfy the demands of field applications such as high hydrogen content, reversibility of hydrogen uptake, and release under moderate conditions. Among the various forms of hydrogen storage such as liquid hydrogen, compressed hydrogen, physisorption on large surface materials (e.g., carbon nanotubes), and lightweight complex hydrides (e.g., alkali metal alanates or borohydrides), it is the lightweight complex hydrides, owing to their high volumetric and gravimetric capacities for hydrogen (95 kg H_2 m^3 and 7.4 wt.% for $NaAlH_4$, respectively), that are considered promising candidates for on-board hydrogen applications [1,2].

Complex hydrides do not reversibly absorb and desorb hydrogen under moderate conditions without an appropriate catalyst. In the late 1990s, it was found that, under moderate conditions of temperature and pressure, $NaAlH_4$, Na_3AlH_6, and Na_2LiAlH_6 when catalyzed by Ti exhibit reversible hydrogen storage characteristics and enhance the kinetics of hydrogen sorption reactions. Ever since then, achieving such reversibility by applying the appropriate catalysts to complex hydrides has been recognized as a key technology [3]. Although Ti halides significantly improve the hydrogen desorption/absorption kinetics of $NaAlH_4$, their addition reduces significantly the hydrogen capacity of $NaAlH_4$ due to the formation of Na halides as reaction products between $NaAlH_4$ and Ti halide during the milling process [4]. The reduction in hydrogen storage capacity during ball milling and/or hydrogen cycling is a drawback of Ti halide-catalyzed $NaAlH_4$. In addition, the formation of a $TiAl_3$ intermetallic compound degrades the catalytic effect of Ti during the hydrogen desorption and absorption processes and this leads to poor cycling stability [5–7]. Therefore, there have been concerted efforts to find new effective catalysts that enhance the sorption kinetics while maintaining the hydrogen capacity at as high a level as possible [8–11].

Recently, Kastel et al. [12,13] reported that TiN nanopowder with high specific surface areas (>200 m^2 g^{-1}) produced by the ammonolysis of solid $TiCl_4$ complexes dramatically improved the hydrogen sorption kinetics of $NaAlH_4$. Bogdanović et al. [14] also demonstrated the enhanced hydrogen absorption rate of $NaAlH_4$ with 2 mol% TiN nanopowder. They reported a sustained stability of hydrogen absorption rate of $NaAlH_4$. It is also remarkable that the hydrogen capacity of $NaAlH_4$ catalyzed with 2 mol% TiN nanopowder was maintained at ~5 wt.% H_2 which, even after a 17 cycletest,

* Corresponding author. Tel.: +82 2 958 6760; fax: +82 2 958 5379.
E-mail address: jhshim@kist.re.kr (J.-H. Shim).

0378-7753/$ – see front matter © 2009 Elsevier B.V. All rights reserved.
doi:10.1016/j.jpowsour.2009.02.083

is close to the theoretical capacity of the catalyzed $NaAlH_4$ (5.6 wt.% H_2), although the reasons were not discussed in detail.

In this study, TiN nanopowder is synthesized by a mechano-chemical route and its catalytic effect on the hydrogen desorption kinetics of $NaAlH_4$ is investigated. The focus is on the characterization of the stability of TiN nanopowder added to $NaAlH_4$ during the hydrogen desorption using in situ X-ray diffraction (XRD) and Raman spectroscopy. Based on these experimental results, the excellent catalytic effects of TiN nanopowder on $NaAlH_4$ are discussed. For comparison, study is made of the catalytic effects of TiB_2 nanopowder, previously synthesized by the mechano-chemical process [15], and $TiCl_3$ commonly used as a catalyst for $NaAlH_4$.

2. Experimental

2.1. Synthesis of TiN nanopowder

Among various synthetic routes to prepare nanostructured materials, mainly through solid-state reactions, mechano-chemical synthesis by high-energy ball milling has been recognized as an effective- and simple way of producing nanocrystalline, amorphous, and other non-equilibrium nanostructured powders [16]. In particular chloride-mediated mechano-chemical reactions have been very effective in producing metallic- and inorganic nanoparticles with homogeneous distribution and uniform particle size [17]. In our previous study [15], we synthesized nanometer-sized TiB_2 particles by a LiCl-mediated mechano-chemical reaction between $LiBH_4$ and $TiCl_3$.

TiN nanopowder was synthesized from $TiCl_3$ (99%) and Li_3N (99%) supplied by Sigma–Aldrich. A mixture of the raw materials was prepared with molar ratios corresponding to the following reaction:

$$TiCl_3 + Li_3N \rightarrow TiN + 3LiCl \quad (1)$$

LiCl (Fluka, 99%) was added to the raw materials as a process control agent. To avoid an excessive increase in temperature during milling, the volume fraction of LiCl in the reaction products would have to be about 90%. Therefore, three grams of each mixture were changed into a hardened-steel vial (internal volume of 150 ml) that was sealed with an O-ring under an argon atmosphere in a glove-box. WC-Co balls, 9 mm in diameter, were used as the milling media and the ball-to-powder weight ratio (BPR) was maintained at approximately 30:1. High-energy ball milling was carried out for 4 h continuously using a planetary ball mill (Retsch PM 200) at a rotation speed of 500 rpm. To remove the LiCl initially added and that produced as a byproduct of reaction (1), the as-milled powder was rinsed several times in distilled water, ethanol and acetone. Following that treatment the powder was recovered from the slurries by means of filtration with cellulose acetate membrane filters (average pore size of 0.1 μm). The TiN powder so recovered was dried for a day in a vacuum oven at ambient temperature. The phase composition of the synthesized TiN powder was analyzed by X-ray diffraction (XRD) using Cu Kα radiation (Bruker D8 Advance). The average crystallite size was estimated using the Scherrer formula [18]. The particle morphology and size distribution were analyzed by transmission electron microscopy (TEM) (FEI TECNAI G^2 F20) that was operated at 200 kV. Using the Digital Micrograph Ver. 3.10.0 (Gatan) program, a fast Fourier transform (FFT) pattern of the high-resolution TEM (HRTEM) image was obtained.

2.2. Characterization of hydrogen sorption properties

Mixtures of $NaAlH_4$ (Sigma–Aldrich, ~97%) and 2 mol% catalysts (TiN, TiB_2 nanopowders and $TiCl_3$) were prepared. Together with four Cr-steel balls of 12.7 mm diameter (each 8.36 g) and fifteen balls of 7.9 mm diameter (each 2.04 g), 1.5 g of each of the above two mixtures were charged into a hardened-steel vial under an argon atmosphere in a glove box and then milled in a Fritch planetary mill (P7) for 2 h at 500 rpm. The thermal decomposition behaviour (hydrogen desorption) of the milled samples was analyzed by a Netzsch 204 F1 Phoenix differential scanning calorimeter (DSC). About 5 mg of the sample were sealed into an aluminum pan with a lid and placed inside the glove-box, and three pinholes were made just before the start of measurement. The rates of heating and of the argon (99.9999%) flow were 5 K min^{-1} and 50 ml min^{-1}, respectively. The hydrogen desorption behaviour and capacities of the samples were also analyzed by thermogravimetry (TG) using Netzsch TG 209 equipment. The heating rate employed was 5 K min^{-1} and the flow rate of 99.9999% argon gas was 50 ml min^{-1}. The consecutive cycles of hydrogen desorption and absorption of $NaAlH_4$ with the catalysts were performed in Sievert-type apparatus for 4 h at 150 °C under 1 bar hydrogen and at 120 °C under 90 bar hydrogen, respectively.

2.3. Stability of TiN nanopowder in $NaAlH_4$

To characterize the stability of TiN nanopowder in $NaAlH_4$ during hydrogen desorption, in situ XRD and Raman spectroscopy measurements were performed. X-ray diffraction patterns were collected with a VÅNTEC-1 detector the featured fast simultaneous recording, which was adequate for in situ investigation. The powder samples were filled in quartz capillary tubes (1 mm o.d., 0.98 mm i.d.) in an argon-filled glove-box and were mounted on a sample support constructed of Swagelok tube fittings. $NaAlH_4$ with a 10 mol% TiN sample was heated in a high-temperature capillary furnace equipped with X-ray transparent windows (MRI Physikalische Geräte GmbH). The heating rate was set at 2 K min^{-1}. A 2θ scan range of 28–58° covered most of the characteristic diffraction peaks of the sample. The scan speed was maintained at 0.8° min^{-1}.

Raman spectra were obtained in backscattering geometry using a Renishaw Ramascope 2000 (Renishaw plc, Gloucestershire, UK) with a spectral resolution of 1 cm^{-1}, and a Linkam THMS600 cell (Linkam Scientific Instruments, UK) directly adapted to the microscope of the instrument; the cell allowed the use of controlled atmosphere and temperature. For more details about the Raman experimental set-up, refer to Borgschulte et al. [19].

3. Results and discussions

3.1. Thermodynamic analysis

Understanding the thermodynamic stability of catalysts in hydrogen storage materials is important in terms of hydrogen storage capacity as well as the stability of the catalytic effect. As already mentioned earlier, it is well known [4] that a transition metal halide catalyst spontaneously reacts with alkali metal complex hydrides during milling. Alkali metal halide is formed and eventually reduces the hydrogen storage capacity of the alkali metal complex hydride. To confirm whether the catalysts remain thermodynamically stable in $NaAlH_4$, thermodynamic equilibrium calculations of $NaAlH_4$ with 2 mol% TiN catalyst and $NaAlH_4$ with 2 mol% TiB_2 catalyst at 25 °C and 1 bar were carried out using the Thermo-Calc program [20]. Gibbs free energy data of all the phases belonging to the Na–Al–H–Ti–N and Na–Al–H–Ti–B systems were taken from the SGTE substance database [21], except for those of $NaAlH_4$ and Na_3AlH_6, which were recently optimized [22]. The calculated results predicted that TiN reacts with $NaAlH_4$ to form AlN and $TiAl_3$, while TiB_2 reacts with $NaAlH_4$ to form $TiAl_3$ and $NaBH_4$, as shown in Table 1. Our previous study [23] had also predicted that $TiCl_3$ reacts with $NaAlH_4$ to form NaCl and $TiAl_3$. Based on thermodynamics, 87, 92, and 92% of the $NaAlH_4$ was expected to remain in the reactions

Table 1
Calculated equilibrium phase fractions of $NaAlH_4$–2 mol% TiN and $NaAlH_4$–2 mol% TiB_2 at 25 °C and 1 bar. Equilibrium phase fraction of $NaAlH_4$–2 mol% $TiCl_3$ taken from Ref. [23].

Phase	$NaAlH_4$–2 mol% TiN	$NaAlH_4$–2 mol% TiB_2	$NaAlH_4$–2 mol% $TiCl_3$
$NaAlH_4$	0.8716	0.9192	0.916
Na_3AlH_6	0.0676	0.0168	0.025
AlN	0.0068	0	0
$TiAl_3$	0.0135	0.0135	0.013
$NaBH_4$	0	0.0404	0
NaCl	0	0	0.010
H_2 (g)	0.0405	0.0101	0.036

of $NaAlH_4$–2 mol% TiN, $NaAlH_4$–2 mol% TiB_2, and $NaAlH_4$–2 mol% $TiCl_3$, respectively, which implies that the gravimetric hydrogen capacity of $NaAlH_4$ with TiN might be the lowest during hydrogen desorption.

3.2. Mechano-chemical synthesis of TiN nanopowder

Fig. 1(a) shows an XRD pattern of the as-milled powder after ball milling for the TiN synthesis indicating that LiCl (space group: $Fm\bar{3}m$, $a = 5.143$ Å, ICSD#: 027981) is present as the major phase. The TiN phase can also be identified in this pattern, although its peak intensities are relatively weak (16% of the maximum intensity) due to the large volume fraction of LiCl. Fig. 1(b) shows an XRD pattern of the rinsed powder without LiCl. The broad peaks of TiN (space group: $Fm\bar{3}m$, $a = 4.238$ Å, ICSD#: 064909) are clearly observed after rinsing. Since no phases other than those of TiN are present, it is concluded that reaction (1) is completed during the high-energy ball milling process. From the FWHM (full-width half-maximum) of the TiN peaks, the average crystallite size of TiN estimated by the Scherrer equation, taking into account the instrumental broadening, is about 6 nm.

The morphologies and size distribution of the synthesized TiN nanopowder were investigated by means of HRTEM analysis. Fig. 2(a) shows a bright field TEM image of the synthesized TiN nanopowder after removal of the LiCl phase. As hard agglomerates are rarely observed, the large volume fraction (~90 vol.%) of LiCl in the reaction products effectively prevents direct impingement of nitride particles during ball milling. The HRTEM image (Fig. 2(b)) shows that the TiN particles are single crystals of 5–9 nm size. This observation is in good agreement with the estimated crystallite size obtained from the XRD pattern (~6 nm). The corresponding FFT

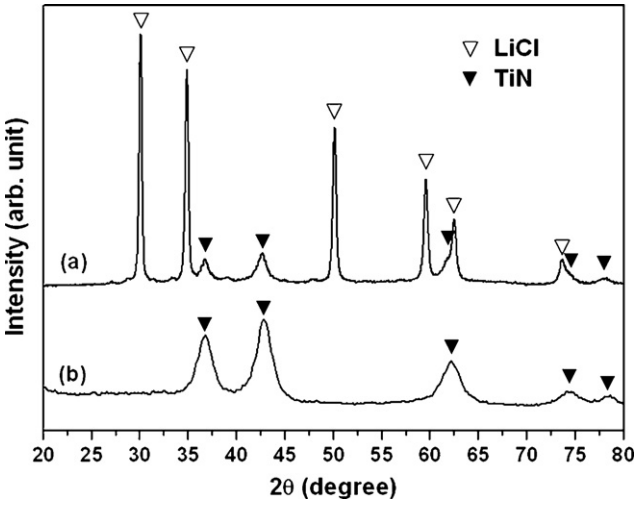

Fig. 1. XRD patterns of powder synthesized according to reaction (1) (a) before and (b) after rinsing.

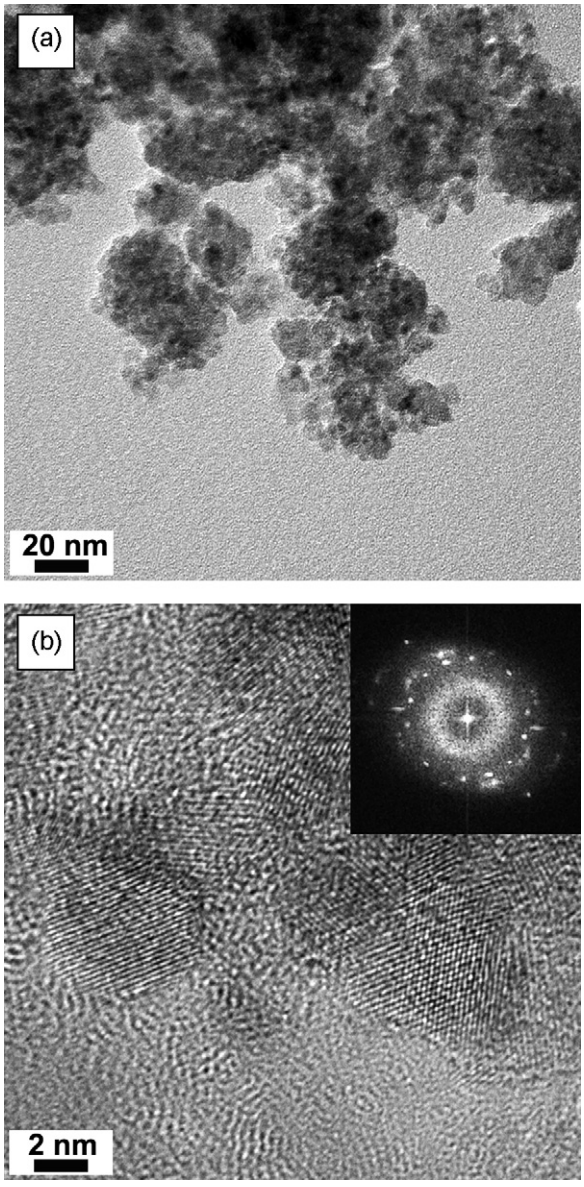

Fig. 2. TEM micrographs of synthesized TiN nanopowder; (a) low magnification and (b) high resolution image. An inset in (b) represents a FFT pattern.

pattern (inset in Fig. 2(b)) of the HRTEM lattice fringes, which can be indexed mainly as (1 1 1) planes (d-spacing: 2.447 Å) and (2 0 0) planes (d-spacing: 2.119 Å) of face-centered-cubic TiN, appears very clear and bright and there by confirms the good crystalline quality of the synthesized TiN nanopowder. The size distribution of the TiN nanopowder is narrow, which is due to the control of size distribution and homogeneity of the particles by addition of the diluent phase (LiCl) during the mechano-chemical reaction [17].

3.3. Catalytic effect of TiN on hydrogen desorption from $NaAlH_4$

To investigate the catalytic effect of as-synthesized TiN and TiB_2 [15] nanopowders, $NaAlH_4$ was mixed with 2 mol% TiN and TiB_2 nanopowders by means of high-energy ball milling. In addition, $NaAlH_4$ was milled under the same milling conditions with 2 mol% TiN- and TiB_2 micron-sized powders (~10 μm), commercial products obtained from Sigma–Aldrich, to confirm whether there is a size effect for the different catalysts. The thermal decomposition (dehydrogenation) behaviour of $NaAlH_4$ with catalysts were characterized by the DSC curves shown in Fig. 3. $NaAlH_4$ desorbs hydrogen

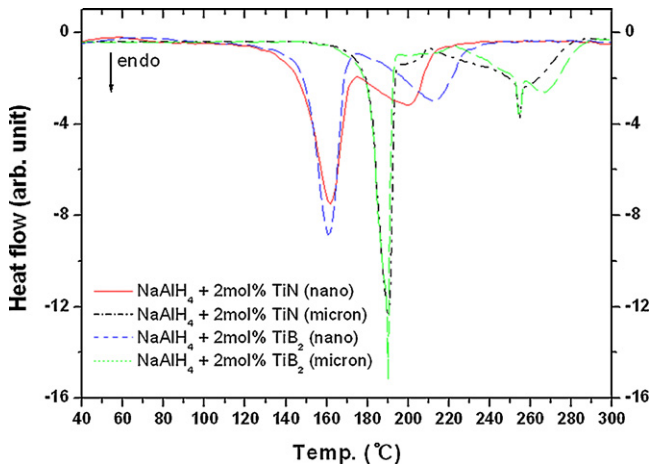

Fig. 3. DSC curves of $NaAlH_4$ with 2 mol% TiN and TiB_2 powders (micron-sized and nano-sized).

in the following two-step reaction [24]:

$$NaAlH_4 \rightarrow \tfrac{1}{3}Na_3AlH_6 + \tfrac{2}{3}Al + H_2 \quad (3.7\,wt.\%\,H_2) \qquad (2a)$$

$$\tfrac{1}{3}Na_3AlH_6 \rightarrow NaH + \tfrac{1}{3}Al + \tfrac{1}{2}H_2 \quad (1.9\,wt.\%\,H_2) \qquad (2b)$$

The two endothermic peaks in the DSC curves correspond to these two steps. For $NaAlH_4$ with 2 mol% TiN nanopowder, the first step (reaction (2a)) starts with the decomposition of $NaAlH_4$ at about 125 °C. Before the first step is complete, the second step (reaction (2b)) starts and is completed at about 220 °C. Although the dehydrogenation start temperature is slightly higher than that of $NaAlH_4$ with $TiCl_3$ [23], the temperature range for the dehydrogenation ($\Delta T = \sim 90$ °C) is narrower than that of $NaAlH_4$ with $TiCl_3$ ($\Delta T = \sim 110$ °C). On the other hand, $NaAlH_4$ with TiB_2 nanopowder begins to decompose at almost the same temperature, but the dehydrogenation reaction is complete at a higher temperature than that of $NaAlH_4$ with TiN nanopowder. The dehydrogenation of $NaAlH_4$ with TiN and TiB_2 micron-sized powders occurs 30–60 °C above that of $NaAlH_4$ with the TiN and TiB_2 nanopowders. It is likely that the higher surface area of the nanopowders improves the dehydrogenation kinetics of $NaAlH_4$ compared with those with the micron-sized powders.

The TG curves in Fig. 4 provide information on the amount of desorbed hydrogen, as well as on the dehydrogenation temperature range. $NaAlH_4$ with $TiCl_3$ releases about 4.8 wt.% hydrogen in the dehydrogenation temperature range between 120 and 230 °C. As

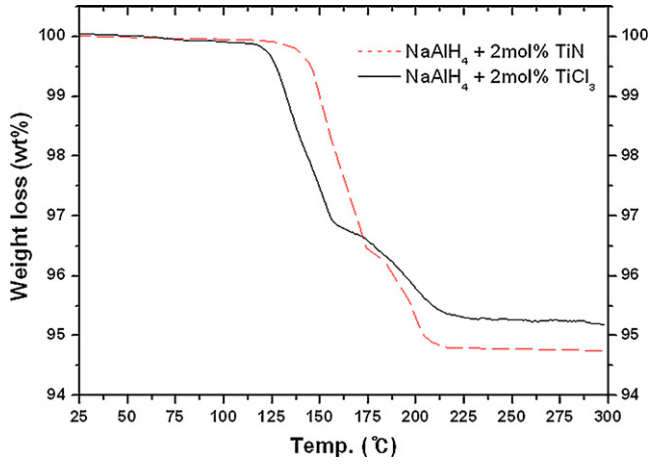

Fig. 4. TG curves of $NaAlH_4$ with 2 mol% $TiCl_3$ and TiN nanopowder.

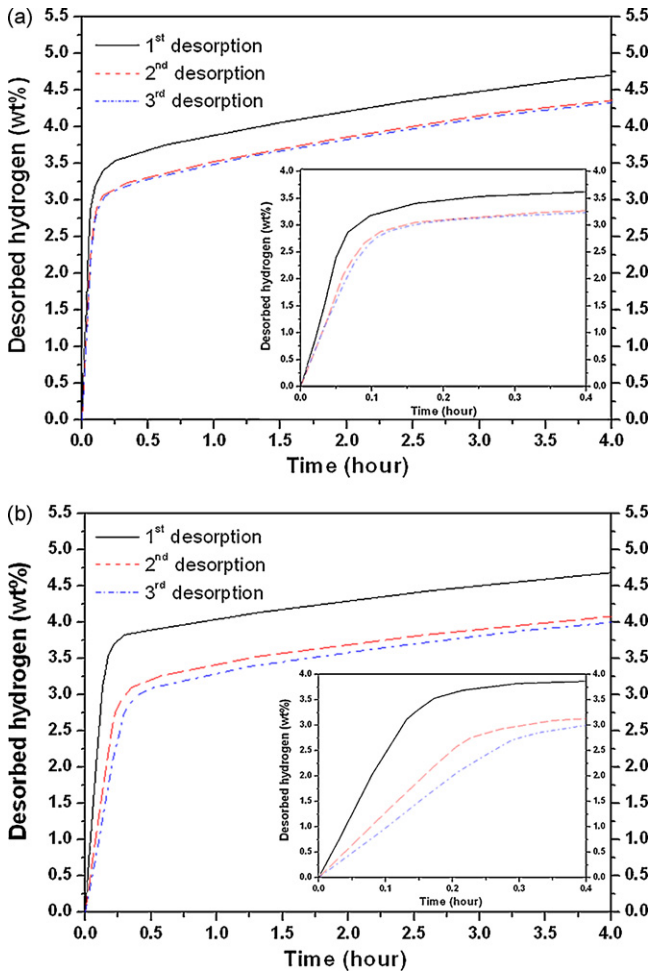

Fig. 5. Hydrogen desorption curves of $NaAlH_4$ with (a) 2 mol% TiN nanopowder and (b) 2 mol% TiB_2 nanopowder during desorption cycles at 150 °C under 1 bar hydrogen. Each inset magnifies the initial hydrogen desorption performance.

mentioned previously, the change in slope at about 150 °C reflects the two-step reaction. The desorbed hydrogen capacity is significantly lower than the theoretical capacity of 5.6 wt.%, because $NaAlH_4$ reacts with $TiCl_3$ to decompose partially during milling. $NaAlH_4$ with TiN nanopowder starts to desorb hydrogen from about 125 °C, which is about 10 °C higher than the dehydrogenation start temperature of $NaAlH_4$ with $TiCl_3$. Note, however that the dehydrogenation reaction of $NaAlH_4$ with TiN nanopowder is completed at about 210 °C, which is about 20 °C lower than the dehydrogenation completion temperature of $NaAlH_4$ with $TiCl_3$. The DSC and TG results indicate that TiN nanopowder is effective, particularly in improving the kinetics of the second-step dehydrogenation reaction (reaction (2b)) of $NaAlH_4$. In addition, $NaAlH_4$ with TiN nanopowder eventually releases more than 5.2 wt.% hydrogen, which is larger than the hydrogen capacity of $NaAlH_4$ with various catalysts reported in the literature [3,4,9,10]. It is remarkable that $NaAlH_4$ with TiN releases more hydrogen than $NaAlH_4$ with $TiCl_3$, although our thermodynamic calculation predicts the reverse. This implies that TiN does not significantly react with $NaAlH_4$ during the milling process, in contradiction with the thermodynamic predictions.

Fig. 5 shows hydrogen desorption curves of $NaAlH_4$ with 2 mol% TiN (Fig. 5(a)) and TiB_2 nanopowders (Fig. 5(b)) at 150 °C under 1 bar hydrogen, measured by Sievert-type apparatus during three cycles. The inset in each figure is a magnification of the initial hydrogen desorption. In Fig. 5(a), $NaAlH_4$ with 2 mol% TiN nanopowder

has remarkably fast desorption kinetics up to 5 min during the first desorption which corresponds to the first-step reaction of $NaAlH_4$ (reaction (2a)) with a hydrogen release of about 3.2 wt.%. The hydrogen desorption rate falls drastically after 5 min and releases about 4.7 wt.% hydrogen in 4 h. This sudden change in dehydrogenation kinetics reflects the transition from reaction (2a) to (2b) of $NaAlH_4$, as described in the DSC and TG results (Figs. 3 and 4). Although the first-cycle desorption rate of reaction (2a) is slightly lower than that of $NaAlH_4$ with $TiCl_3$, the rates for the second- and third hydrogen desorption cycles exceed those of $NaAlH_4$ with $TiCl_3$ (see Fig. 4(a) in Ref. [23]). Moreover, there is only a small degradation in the desorption rate of reaction (2a) over three cycles and the amount of desorbed hydrogen is larger than that of $NaAlH_4$ with $TiCl_3$; 4.3–4.7 wt.% hydrogen is released in 4 h. For comparison, the desorption kinetics of $NaAlH_4$ with 2 mol% TiB_2 nanopowder was also measured. As can be seen in Fig. 5(b), the first desorption kinetics of $NaAlH_4$ with 2 mol% TiB_2 nanopowder are slightly slower than those of $NaAlH_4$ with 2 mol% TiN nanopowder, although the former desorbs slightly more hydrogen through reaction (2a). During the second and third hydrogen-desorption cycles, the kinetics of reaction (2a) degrade significantly compared with the first desorption. In addition, the quantity of desorbed hydrogen declines to about 4.0 wt.% with cycling.

In summary the TiN nanopowder synthesized in this study exhibits a better catalytic effect on the cyclability and hydrogen capacity of $NaAlH_4$ than the well-known $TiCl_3$ catalyst. Nevertheless, for TiN nanopowder to be seriously considered as an alternative catalyst to $TiCl_3$ for hydrogen storage in $NaAlH_4$, further studies of the hydrogen absorption kinetics and the long-term cycling stability of TiN-catalyzed $NaAlH_4$ are required.

3.4. *In situ XRD analysis*

As mentioned above and has been described in the work of Bogdanović et al. [14], the most encouraging feature of TiN nanopowder as a catalyst is that the reduction in hydrogen capacity of $NaAlH_4$ is relatively small during hydrogen sorption cycling. The sustained hydrogen capacity seems to be associated with the stability of the TiN nanopowder in $NaAlH_4$. To verify this possibility, in situ XRD measurements were performed at temperatures ranging from 30 to 220 °C at a heating rate of 2 K min^{-1} under 1 bar of hydrogen. For these measurements, a ball-milled sample of $NaAlH_4$ with excess of TiN nanopowder (~10 mol%) was prepared with the aim of detecting the TiN phase clearly in the X-ray diffraction pattern.

Fig. 6(a) shows XRD patterns obtained during hydrogen desorption of $NaAlH_4$ with TiN nanopowder. As can be seen in Fig. 6(a), the first step of the decomposition of $NaAlH_4$ (reaction (2a)) starts between 120 and 140 °C, is accompanied by the appearance of the Na_3AlH_6 and Al phases, and finishes at the middle of the 160 °C segment. The NaH phase, which indicates the decomposition of Na_3AlH_6 (reaction (2b)), appears in the diffraction patterns in the middle of the 150 °C segment and reaction (2b) is completed at around 210 °C. The XRD patterns corresponding to each hydrogen desorption step of the TiN-catalyzed $NaAlH_4$ are in good agreement with the DSC and TG results.

Selected XRD patterns at each temperature are shown in Fig. 6(b). At room temperature, the catalyzed $NaAlH_4$ phase can be indexed as a reference (space group: $I4_1/a$, a = 5.021 Å, c = 11.346 Å, ICSD#: 020923); therefore, it can be inferred that there is no interaction between TiN and $NaAlH_4$, such as the substitution of Na or Al by Ti, which might have resulted in a peak shift in the XRD patterns. With rise in temperature, the peaks of $NaAlH_4$ shift to lower 2θ values due to thermal expansion [25]. After the start of decomposition of $NaAlH_4$ at around 140 °C, the phases produced are indexed as follows: Na_3AlH_6 (space group: $P2_1/n$, a = 5.460 Å, b = 5.610 Å, c = 7.800 Å, β = 90.18°, PDF#: 201072), Al (space group: $Fm\bar{3}m$, a = 4.049 Å, ICSD#: 064700), and NaH (space group: $Fm\bar{3}m$, a = 4.890 Å, ICSD#: 033670). The final products after decomposition (220 °C) of $NaAlH_4$ with 10 mol% TiN are NaH, Al and TiN, as expected.

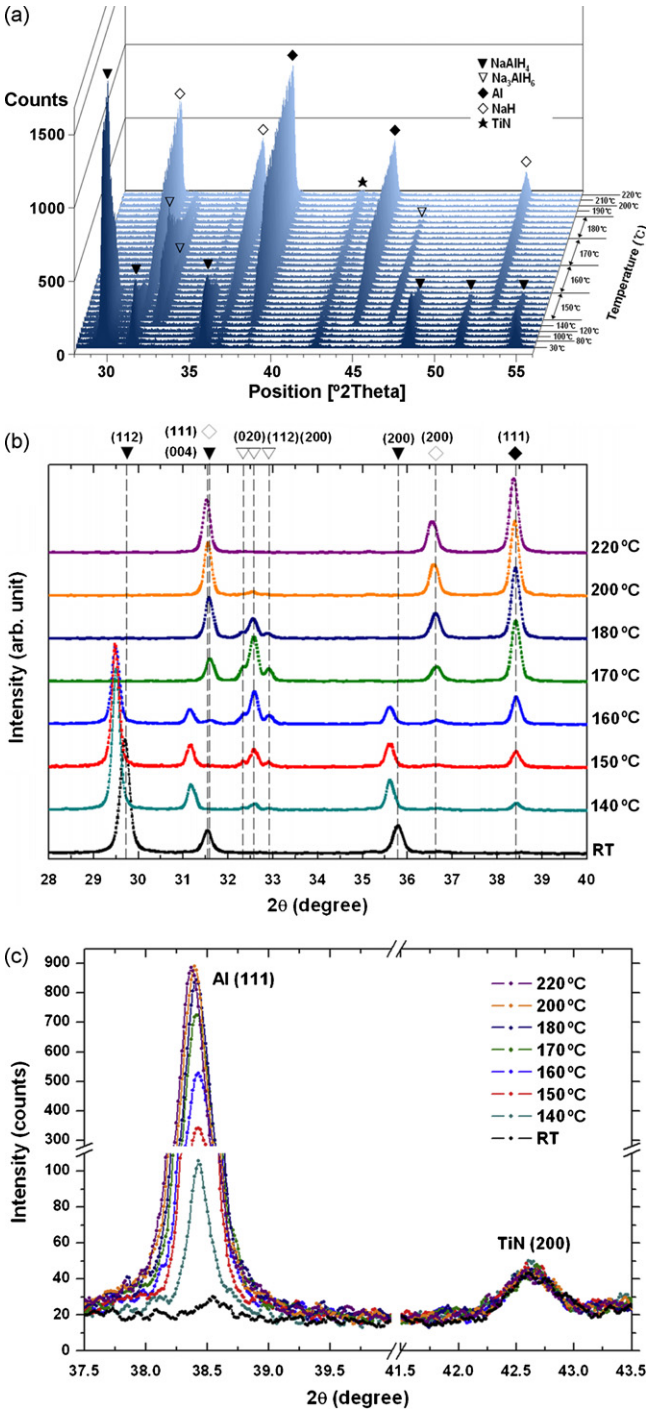

Fig. 6. In situ XRD patterns recorded during hydrogen desorption of $NaAlH_4$ with 10 mol% TiN nanopowder; (a) whole XRD patterns during hydrogen desorption, (b) selected XRD patterns covering the $NaAlH_4$, Na_3AlH_6, NaH and Al, (c) enlarged part of Al (1 1 1) and TiN (2 0 0) diffraction.

From previous XRD results [6,26,27], the catalysis of $NaAlH_4$ with $TiCl_3$ resulted in asymmetrical broadening of the Al peak towards the high-angle side, which indicates the formation of a $TiAl_x$ intermetallic compound (likely $TiAl_3$) during the ball milling process or the hydrogen sorption cycle, even at low temperatures. Balde et al. [7] proposed a ranking of the catalytic activity of the Ti cata-

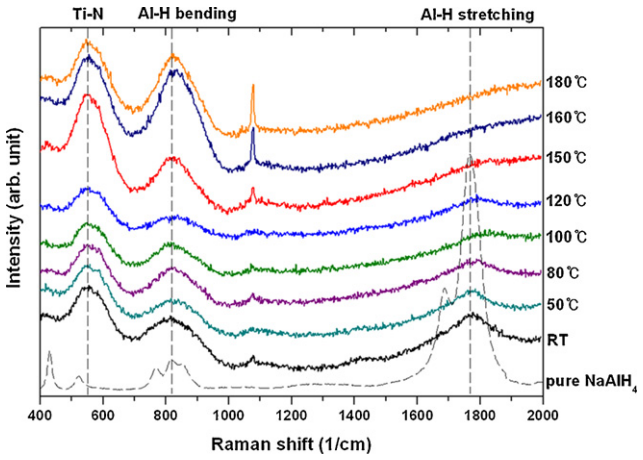

Fig. 7. In situ Raman spectra measured during hydrogen desorption of $NaAlH_4$ with 10 mol% TiN nanopowder.

lyst for the hydrogen sorption of $NaAlH_4$ as follows: Ti in the Al surface > $TiAl_3$ cluster > $TiAl_3$ crystalline. Hence, the best catalytic effect appears when the distance between Ti and Al is maintained as close as possible without producing any intermetallic compounds. In Fig. 6(c), a magnification of the selected XRD patterns is presented in order to enable examination of the symmetry of the Al main peak (1 1 1) and of the stability of the TiN phase. The diffraction peak of Al maintains its symmetrical shape even after complete desorption of hydrogen at 220 °C, although the peak intensity of Al increases during the hydrogen desorption. This implies that there is no formation of a $TiAl_x$ intermetallic compound, which was observed with $TiCl_3$ as the catalyst. It is also worth noting that the main diffraction peak of the TiN phase (2 0 0) remains without significant change in the position, intensity and broadening of the peak during the whole in situ XRD measurement process. From these results, it can be inferred that there are no reaction products between TiN nanopowder and $NaAlH_4$ such as the AlN and $TiAl_3$ phases that were predicted by thermodynamic calculation.

3.5. *In situ Raman spectroscopy analysis*

To confirm the stability and the catalytic effect of the TiN catalyst, in situ Raman spectroscopy analysis was performed during the hydrogen desorption of $NaAlH_4$ with 10 mol% TiN nanopowder under 1 bar of hydrogen. Information about the Ti–N bonding of TiN and the Al–H bonding of $NaAlH_4$ is noted in Fig. 7. The Raman spectrum of $NaAlH_4$ obtained at room temperature is in good agreement with pure $NaAlH_4$ as well as the previous results [19,28–30] at around 810 cm^{-1} (Al–H bending mode) and 1780 cm^{-1} (Al–H stretching mode), although there is broadening of the peak caused by the catalyst and ball milling [19,30]. Ti–N bonding (550 cm^{-1} [31]) is also clearly identified in the spectrum at room temperature. With increase in temperature, the intensities of Al–H bonding (both bending and stretching modes) show a gradual decrease up to 120 °C, which is exactly the starting point of decomposition of TiN-catalyzed $NaAlH_4$ measured by DSC and TG. On the other hand, the general peak shift of Al–H stretching modes to higher frequency (1801 cm^{-1}) is not clearly discernible due to peak broadening and the weak intensity. Between 120 and 145 °C, the intensity of peaks in the region from 700 to 1000 cm^{-1} recovers, whereas the Al–H stretching mode of $NaAlH_4$ disappears completely. From a previous study [19], it can be inferred that this signal is related to the formation of Na_3AlH_6 through reaction (2a). The chemical bonding of Ti–N clearly implies that the TiN catalyst remains chemically stable through the whole hydrogen desorption process. These Raman spectra confirm once again the stability of the TiN catalyst. The sharp peak around 1080 cm^{-1} seems to arise from impurities.

4. Conclusions

In this study, TiN nanopowder is synthesized through a novel method using a mechano-chemical reaction. The TiN nanopowder consists of single-crystal particles with an average size of 6 nm. A study has been made of the use of $NaAlH_4$ as a catalyst for hydrogen sorption reactions. In comparison with $TiCl_3$ and TiB_2 nanopowder catalysts, $NaAlH_4$ with TiN nanopowder display improved hydrogen desorption rates and an enhanced hydrogen capacity close to the theoretical value of pure $NaAlH_4$. In contrast to the nanopowders, micron-sized TiN and TiB_2 powders hardly exhibit a catalytic effect on the hydrogen desorption of $NaAlH_4$. In situ XRD and Raman spectroscopy studies reveal that the TiN nanopowder remains stable during the milling and dehydrogenation processes, which might help it maintain its catalytic effect during hydrogen sorption cycles.

Acknowledgments

The study was sponsored by the KIST Core Competence Program and by the Korea Research Foundation Grant funded by the Korean Government (MOEHRD) (KRF-2007-612-D00097).

References

[1] L. Schlapbach, A. Züttel, Nature 414 (2001) 353–358.
[2] S. Orimo, Y. Nakamori, J.R. Eliseo, A. Züttel, C.M. Jensen, Chem. Rev. 107 (2007) 4111–4132.
[3] B. Bogdanović, M. Schwickardi, J. Alloys Compd. 253 (1997) 1–9.
[4] G. Sandrock, K. Gross, G. Thomas, J. Alloys Compd. 339 (2002) 299–308.
[5] S.S. Srinivasan, H.W. Brinks, B.C. Hauback, D. Sun, C.M. Jensen, J. Alloys Compd. 377 (2004) 283–289.
[6] A.G. Haiduc, H.A. Stil, M.A. Schwarz, P. Paulus, J.J.C. Geerlings, J. Alloys Compd. 393 (2005) 252–263.
[7] C.P. Balde, H.A. Stil, A.M.J. van der Eerden, K.P. de Jong, J.H. Bitter, J. Phys. Chem. C 111 (2007) 2797–2802.
[8] X.Z. Ma, E. Martinez-Franco, M. Dornheim, T. Klassen, R. Bormann, J. Alloys Compd. 404–406 (2005) 771–774.
[9] B. Bogdanović, M. Felderhoff, A. Pommerin, F. Schüth, N. Spielkamp, Adv. Mater. 18 (2006) 1198–1201.
[10] G.-J. Lee, J.-H. Shim, Y.W. Cho, K.S. Lee, Int. J. Hydrogen Energy 32 (2007) 1911–1915.
[11] K.S. Jung, D.H. Kim, E.Y. Lee, K.S. Lee, Catal. Today 120 (2007) 270–275.
[12] S. Kastel, K. Schlichte, G. Chaplais, M. Khanna, J. Mater. Chem. 13 (2003) 1496–1499.
[13] S. Kaskel, K. Schlichte, T. Kratzke, J. Mol. Catal. A 208 (2004) 291–298.
[14] B. Bogdanović, M. Felderhoff, S. Kaskel, A. Pommerin, K. Schlichte, F. Schüth, Adv. Mater. 15 (2003) 1012–1015.
[15] J.W. Kim, J.-H. Shim, J.-P. Ahn, Y.W. Cho, J.-H. Kim, K.H. Oh, Mater. Lett. 62 (2008) 2461–2464.
[16] C. Suryanarayana, Prog. Mater. Sci. 46 (2001) 1–184.
[17] T. Tsuzuki, P.G. McCormick, J. Mater. Sci. 39 (2004) 5143–5146.
[18] B.D. Cullity, S.R. Stock, Elements of X-ray diffraction, third ed., Prentice Hall, London, 2001.
[19] A. Borgschulte, A. Züttel, P. Hug, G. Barkhordarian, N. Eigen, M. Dornheim, R. Bormann, A.J. Ramirez-Cuesta, Phys. Chem. Chem. Phys. 10 (2008) 4045–4055.
[20] http://www.thermocalc.se.
[21] http://www.sgte.org.
[22] B.-M. Lee, J.-W. Jang, J.-H. Shim, Y.W. Cho, B.-J. Lee, J. Alloys Compd. 424 (2006) 370–375.
[23] G.-J. Lee, J.-H. Shim, Y.W. Cho, K.S. Lee, Int. J. Hydrogen Energy 33 (2008) 3748–3753.
[24] K.J. Gross, G.J. Thomas, C.M. Jensen, J. Alloys Compd 330–332 (2002) 638.
[25] K.J. Gross, S. Guthrie, S. Takara, G. Thomas, J. Alloys Compd. 297 (2000) 270–281.
[26] B. Bogdanovic, M. Felderhoff, M. Germann, M. Hartel, A. Pommerin, F. Schuth, C. Weidenthaler, B. Zibrowius, J. Alloys Compd. 350 (2003) 246–255.
[27] H.W. Brinks, C.M. Jensen, S.S. Srinivasan, B.C. Hauback, D. Blanchard, K. Murphy, J. Alloys Compd. 376 (2004) 215–221.
[28] H. Yukawa, N. Morisaku, Y. Li, K. Komiya, R. Rong, Y. Shinzato, R. Sekine, M. Morinaga, J. Alloys Compd. 446–447 (2007) 242–247.
[29] E.H. Majzoub, K.F. McCartny, V. Ozolins, Phys. Rev. B 71 (2005) 024118.
[30] S. Gomes, G. Renaudin, H. Hagemann, K. Yvon, M.P. Sulic, C.M. Jensen, J. Alloys Compd. 390 (2005) 305–313.
[31] W. Spengler, R. Kaiser, Solid State Commun. 17 (1975) 19–22.